Available online at www.sciencedirect.com

ScienceDirect

Scripta Materialia 76 (2014) 53–56

Scripta MATERIALIA

www.elsevier.com/locate/scriptamat

Modeling residual porosity in thick components consolidated by spark plasma sintering

J. Milligan,[a] P. Hendrickx,[a] M.M. Tünçay,[a] E.A. Olevsky[b] and M. Brochu[a,*]

[a]*Department of Mining and Materials Engineering, Aluminum Research Centre – REGAL, McGill University, 3610 University St, Montreal, Quebec H3A 0C5, Canada*

[b]*San Diego State University, Powder Technology Laboratory, 5500 Campanile Drive, San Diego, CA 92182-1323, USA*

Received 17 October 2013; revised 20 December 2013; accepted 23 December 2013
Available online 29 December 2013

A constitutive model for densification during spark plasma sintering was adapted and applied to an aluminum–magnesium alloy to determine the effect of increasing sample thickness on residual porosity after sintering. The contributions of electromigration, sintering stresses and external load (on creep, diffusion and yielding) were all taken into consideration, as well as the effect of pressure on increasingly thick components. The results show that the overall description of the spark plasma sintering process agrees with the experimental results.

Keywords: Spark plasma sintering; Aluminum alloys; Sintering; Powder consolidation

Spark plasma sintering (SPS) has, over the past 20 years, come to light as a promising approach for rapid powder consolidation [1,2] and cladding operations [3–5]. This consolidation process involves rapidly heating the powder by electric current along with the simultaneous application of pressure. During compaction, the effective applied pressure within the compact generally decays with increasing thickness [6]. This pressure decay inside the sample is problematic for the fabrication of thicker samples, as it may lead to a gradient of porosity throughout the final microstructure, which would adversely affect the mechanical properties. Hence, prediction and parameter optimization aiming for the removal of any residual porosity in the compact is of paramount importance. The complex nature of the SPS process has led to attempts of modeling the various phenomena occurring during the sintering process [7–10]. Constitutive models have been derived by Olevsky and Froyen [7] describing the effects of electromigration, sintering stress and the external load on diffusion. An attempt is made herein to augment this constitutive model so as to predict the remaining porosity in samples with increasing thicknesses. This will facilitate determining the relationship between thickness and remaining porosity for a given system, and to contribute to the selection of sintering parameters that would allow the elimination of any residual porosity.

Commercial aluminum alloy 5356 powder (composition: 4.5–5.5 wt.% Mg; 0.4 wt.% Fe; 0.25 wt.% Si; 0.1 wt.% Zn; 0.1 wt.% Cu; 0.06–0.2 wt.% Cr, Mn, Ti) was sintered in an ISO-Carb85 graphite die using a Thermal Technology LLC 10-3 spark plasma sintering press. The powder particles were spherical in morphology, having a particle size distribution mean of 28 μm with a standard deviation of 16 μm. The powder was consolidated into pucks of 20 and 38 mm diameter with varying thicknesses. The overall die dimensions were as follows: the height of the smaller die (20 mm) was 40 mm, with a 15 mm wall thickness; and the height of the larger die (38 mm) was 46 mm, with a wall thickness of 17.5 mm. These die cavity sizes then allowed for approximately four times the volume of powder to be placed into the 38 mm diameter die compared to the 20 mm, with a slightly higher wall thickness affecting the thermal load of the sintering cycle. The heating rate was maintained at 100 °C min^{-1}, with a soaking time of 1 min at 500 °C for the 20 mm die and 1 min at 400 °C for the 38 mm die. A mechanical vacuum level of 6.0×10^{-2} torr was maintained prior to and throughout the sintering cycle. Temperature was measured using a C-type thermocouple placed in a hole, drilled to 2 mm from the surface of the sample, in the bottom punch. A preload pressure of 10 MPa by single-action pressing

* Corresponding author. Tel.: +1 514 398 2354; fax: +1 514 398 4492; e-mail: mathieu.brochu@mcgill.ca

1359-6462/$ - see front matter © 2014 Acta Materialia Inc. Published by Elsevier Ltd. All rights reserved.
http://dx.doi.org/10.1016/j.scriptamat.2013.12.014

was applied and was then ramped to the maximum pressure of 50 MPa during the heating stage, which was maintained throughout the holding temperature. Cross-sections of the pucks were ground and polished using 240, 400, 600, 800 and 1200 grit SiC paper, followed by polishing with 3 and 1 micron diamond suspensions and a 0.05 micron colloidal silica suspension. The residual porosity of the sintered pucks was analyzed using a Nikon light optical microscope equipped with a Clemex Vision System. Reported experimental values were averaged from a minimum of 10 image fields across the sample from a minimum of three samples per condition.

The constitutive model, developed by Olevsky and Froyen [7], includes the effects of the external load on creep and grain boundary diffusion, electromigration and sintering stresses. The axial strain rates observed for each densification phenomenon are shown in Eqs. (1)–(4)for the contributions of the external load on creep and grain boundary diffusion, electromigration and sintering stresses, respectively.

$$\dot{\varepsilon}_{crx} = \left[\left(\frac{3\theta}{2}\right)^{\frac{3}{2}}\left(\frac{3\alpha}{2G}(1-\theta)-\sigma_x\right)/A(1-\theta)^{5/2}\right]^{1/m} \tag{1}$$

$$\dot{\varepsilon}^{load}_{gbx} = \frac{\delta_{gb}D_{gb}}{kT}\frac{\Omega}{G+r_p}\frac{\sigma_x}{G^2} \tag{2}$$

$$\dot{\varepsilon}^{em}_{gbx} = \frac{\delta_{gb}D_{gb}}{kT}\frac{Z^*q_e}{(G+r_p)^2}\frac{U}{l} \tag{3}$$

$$\dot{\varepsilon}^{st}_{gbx} = -\frac{3\delta_{gb}D_{gb}}{kT}\frac{\Omega}{(G+r_p)^2}\frac{\alpha}{G}\left[\frac{1}{r_p}-\frac{1}{2G}\right] \tag{4}$$

where θ is the remaining porosity, $\delta_{gb}D_{gb}$ is the grain boundary diffusion coefficient at a given temperature, Ω is the atomic volume, σ_x is the applied pressure, k is the Boltzmann's constant, T is temperature in kelvin, G is the grain size, which is assumed to be one grain per particle during sintering (i.e. particle size is equal to the grain size), r_p is the pore radius, A is the power-law creep frequency factor, m is the power-law creep exponent, Z^*q_e is the effect charge, U/l is the applied field and α is the surface tension. Values for these parameters can be found in the literature [7]. The overall strain rate observed is the summation of these sintering phenomena shown in Eq. (5).

$$\dot{\varepsilon}_{\text{total}} = \dot{\varepsilon}_{crx} + \dot{\varepsilon}^{em}_{gbx} + \dot{\varepsilon}^{st}_{gbx} + \dot{\varepsilon}^{load}_{gbx} \tag{5}$$

The total strain rate can then be converted to overall densification rate by the following conversion, shown as Eq. (6):

$$\dot{\theta} = (1-\theta)\dot{\varepsilon}_{\text{total}} \tag{6}$$

The overall densification described in Eqs. (1)–(6)does not account for all of the possible effects of applied pressure during densification. Of particular importance to metallic materials is the densification contribution achieved by yielding (assumed to be instantaneous), described by Eq. (7)when the overall density of the compact is less than 90% of the theoretical density (TD) and by Eq. (8)when it is greater than 90% TD [6,11]:

$$\rho_{\text{Yield}} = \left(\frac{(1-\rho_0)\sigma_x}{1.3\sigma_y}+\rho_0^3\right) \quad \rho \leqslant 0.9 \tag{7}$$

$$\rho_{\text{Yield}} = 1-\exp\left(-\frac{3\sigma_x}{2\sigma_y}\right)\rho > 0.9 \tag{8}$$

where ρ_{Yield} is the density achieved due to plastic yielding and ρ_0 is the initial density. As the temperature increases during the ramp, the yield strength of the material will change dramatically. The effect of the temperature on the yield strength σ_y of commercial AA 5356 can be described by the following equation [12] above room temperature, where T is in kelvin:

$$\sigma_{\text{y}} = 20 + \frac{126}{1+10^{-0.0091(525-T)}} \tag{9}$$

Finally, a pressure gradient throughout the sample must be considered when using uniaxial pressing for tall samples, where the applied pressure gradient will change as a function of the total thickness. A rigorous analysis of die-pressing taking into account friction at the die walls, strictly speaking, requires a boundary-value problem formulation. This problem, due to the non-linearity of the constitutive equations, does not allow for an analytical solution and cannot be easily reduced to a set of ordinary differential equations describing the contribution of the applied axial stress to the shrinkage kinetics via plastic yield mass transport mechanism. Therefore, to simplify the problem, we employ an empirical relationship in Eq. (10). In single-action pressing, only one punch moves during pressing, leading to a decrease in effective pressure from the moving punch towards the static punch. The effective pressure σ_{eff} is a function of the thickness x, the diameter of the sample d, the coefficient of friction between the die wall and the powder μ, and the proportionality factor z [6]. In the current study, the friction coefficient was considered constant as a function of temperature, and a value of 0.16 was used for the system, representing Al–graphite [13]:

$$\sigma_{\text{eff}}(x) = \sigma_x \exp\left(-\frac{4\mu z x}{d}\right) \tag{10}$$

The total shrinkage of the compact using the constitutive models developed by Olevsky and Froyen, with the inclusion of the yielding and pressure gradient phenomena, was solved iteratively using MATLAB programming software to determine the remaining porosity as a function of sintered thickness.

Using Eq. (10)to calculate the reduction in effective applied pressure throughout the die, the change in porosity was calculated for samples of various thicknesses. The calculated residual porosity as a function of time for increasing component thicknesses for the 38 mm die is shown in Figure 1. As the thickness of the compact increases, the remaining porosity increases as a result of pressure decay. For this AA5356 alloy, when increasing the thickness of the compact from 5.3 to 28.9 mm, the predicted increase in remaining porosity of the samples rangeed from 5.5 to 6.2%, respectively, as plotted in Figure 2a and b for the 20 and 38 mm die, respectively.

The residual porosity was measured from grayscale thresholding of optical images and plotted as density

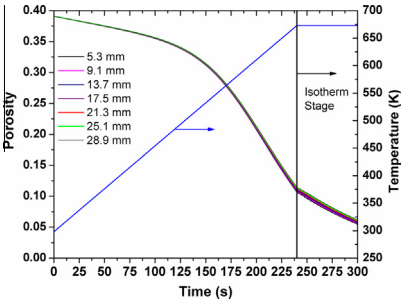

Figure 1. The calculated effect of increasing thickness on the densification of the compact for the 38 mm diameter die.

vs. thickness graphs, as shown in Figure 2a and b for the 20 and 38 mm die, respectively. Due to the height of the die, the maximum thickness achievable for the 20 mm diameter die (Fig. 2a), with this particular powder, was approximately 8 mm (depending on the packing of the powder and the height of the graphite die, which was 40 mm with the current apparatus). After sintering, the measured density of the compact throughout its thickness was uniform and agreed well with the final density predicted by the model. Up to 8 mm of compact thickness, the density was predicted to be 100% of the TD and was measured to be 99.5% of TD throughout the depth of the sample. Due to the increased thermal load in the larger die, a lower temperature was used during testing with the larger die. After sintering at 400 °C for 1 min in the larger die, the density of the compact was also found to be uniform throughout the entirety of the thickness. Any pressure gradients developing in the powder bed are due to the friction between the powder and the face of the die [6], as observed in Eq. (10). The friction coefficient between Al and graphite is low enough to produce very minimal pressure gradients from the top punch to the bottom when pressing thick Al samples, suggesting that samples much greater than

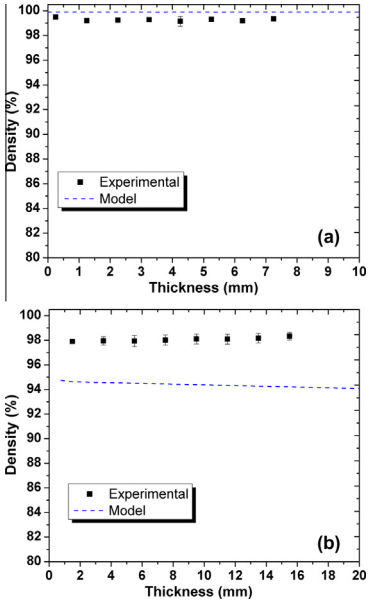

Figure 2. The density measured as a function of sample thickness for (a) the 20 mm diameter die and (b) the 38 mm diameter die. Applied pressure: 50 MPa.

20 mm in thickness could be sintered before a significant drop in porosity is observed. The experimental value for the 38 mm die was approximately 3–4% higher than predicted by the model. The value used in the calculation of the final density is based on the set temperature profile for the sintering run. Because of a large thermal load inside the die, there is expected to be a thermal gradient inside the sample, leading to a higher temperature and increased plasticity, and resulting in the higher density than predicted by the constitutive model. This phenomenon has been shown to exist through finite element analysis of 20 mm dies [14,15], where thermal gradients were shown to be approximately on the order of 10–50 °C, depending on the thermal conductivity of the metal. It is surmised that its effect shall be exacerbated in the larger die, as was shown by Rathel et al. [16] in larger die sizes sintering electrically conductive tungsten carbide. The authors showed that thermal gradients between 40 and 120 °C might be present, depending on the die geometry.

With temperature remaining constant, the density of the final compact greatly depends on the applied pressure during sintering and how effectively the pressure is transmitted throughout the die. As demonstrated in Figure 2b, an applied pressure of 50 MPa is insufficient to achieve full density in the larger 38 mm die under these sintering conditions. An increase in applied pressure was changed in the model and predictions dictate that an increase in pressure by 5 MPa should result in an approximate increase in density of 3%. The increased pressure of 55 MPa was then applied to a sample in the large 38 mm die and the density as a function of thickness was plotted and compared to the predictions by the model at 50 and 55 MPa, as shown in Figure 3. The final density achieved throughout the compact was 100%, and again was 3–4% higher than the predictions of the model. In the present analysis, any thermal gradients that may be present inside the die are not considered in the calculation of the density from the constitutive model. The model correctly predicted the magnitude of density increase that resulted from the extra 5 MPa of pressure, i.e. 3%, while the experimental results showed an increase from 98% up to 100% of the TD. As demonstrated, the densification range is similar, but the absolute density values are slightly off, which is believed to be caused by the presence of a thermal gradient due to the large sample size. In order for the predictions to meet the experi-

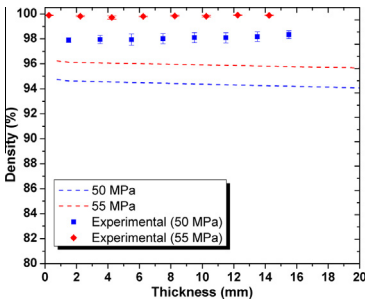

Figure 3. The density as a function of thickness for the 38 mm die for 50 and 55 MPa compared to the predictions by the constitutive model.

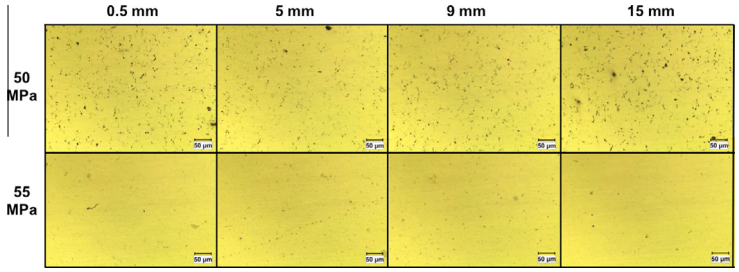

Figure 4. Optical images along the center of the compacts sintered at 50 and 55 MPa for increasing thickness.

ments, an estimate of a thermal gradient of 50 °C in the 38 mm die configuration was found. This higher temperature in the die would allow additional plasticity of the powder, resulting in a prediction meeting the experimental values. This value is of the same order as what has been reported and determined through finite element analysis of the SPS process [14–18].

Micrographs of the samples sintered at 50 and 55 MPa are shown in Figure 4 and confirm the increase in final density with the increase in applied pressure. The density with increasing thickness is extremely uniform, indicating excellent pressure transmission throughout the die, regardless of the size. As previously mentioned, the larger die results in a significantly larger thermal load in the SPS. During the heating process, the larger thermal load will require an increased amount of power to increase the temperature. This increased power application will lead to a larger thermal gradient inside the powder bed, resulting in higher plasticity in the powder bed. As such, the limit in thickness achievable depends on the size of the die and further studies should be done to determine if there exist any limits to the sample thickness. Any thermal gradients will have to be determined empirically (or by finite element analysis) and fitted into the model for a given die dimension.

The constitutive model derived by Olevsky and Froyen [7] was adapted to calculate the final density as the thickness of the sample increased. The model agreed well with the densities measured for a small die of 20 mm diameter. For the 20 mm diameter die, samples up to 8 mm in thickness can be expected to have uniform densities throughout. A larger die (of 38 mm diameter) showed higher experimental values than predicted, which is most likely due to the different thermal gradient characteristics from the larger diameter die. Increasing the pressure applied can help facilitate the increase in the overall density to 100% of the theoretical density. An estimate of the thermal gradient inside the large die was made and was determined to be approximately 50 °C, at which point the model and experimental values agreed well with each other.

The authors thank NSERC, REGAL and McGill (MEDA) for financial support of this research. The support of the San Diego State University researcher by the US Department of Energy, Materials Sciences Division, under Award No. DE-SC0008581 is gratefully acknowledged.

[1] J.E. Garay, in: Annual Review of Materials Research, Palo Alto, CA, Annual Reviews, 2010, pp. 445–468.
[2] Z.A. Munir, D.V. Quach, M. Ohyanagi, J. Am. Ceram. Soc. 94 (2011) 1–19.
[3] L. Limeng, Y. Feng, Z. Yu, Z. Zhiguo, H. Qinglong, J. Eur. Ceram. Soc. 30 (2010) 2683–2689.
[4] T. Nagae, S. Tomida, A. Okada, N. Inada, Surf. Coat. Technol. 169–170 (2003) 174–177.
[5] S. Yoo, J. Groza, T.S. Sudarshan, K. Yamakazi, Scr. Mater. 34 (1996) 1383–1386.
[6] R.M. German, Powder Metallurgy & Particulate Materials Processing, MPIF, Princeton, NJ, 2005, pp. 181–214.
[7] E. Olevsky, L. Froyen, Scr. Mater. 55 (2006) 1175–1178.
[8] E.A. Olevsky, L. Froyen, J. Am. Ceram. Soc. 92 (2009) S122–S132.
[9] E.A. Olevsky, S. Kandukuri, L. Froyen, J. Appl. Phys. 102 (2007), 114913–114912.
[10] J. Ye, L. Ajdelsztajn, J. Schoenung, Metall. Mater. Trans. A 37 (2006) 2569–2579.
[11] H.J. Frost, M. Ashby, Deformation-Mechanism Maps, Pergamon Press, New York, 1982.
[12] J.W. Bray, Properties and Selection: Nonferrous Alloys and Special-Purpose Materials, ASM International, Materials Park, OH, 1991.
[13] B.S. Shabel, D.A. Granger, W.G. Truckner, Friction, Lubrication, and Wear Technology, ASM International, Materials Park, OH, 1992.
[14] U. Anselmi-Tamburini, S. Gennari, J.E. Garay, Z.A. Munir, Mater. Sci. Eng. A 394 (2005) 139–148.
[15] D. Tiwari, B. Basu, K. Biswas, Ceram. Inter. 35 (2009) 699–708.
[16] J. Rathel, M. Herrmann, W. Beckert, J. Eur. Ceram. Soc. 29 (2009) 1419–1425.
[17] K. Vanmeensel, A. Laptev, J. Hennicke, J. Vleugels, O. Van der Biest, Acta Mater. 53 (2005) 4379–4388.
[18] Y. Wang, Z. Fu, Mater. Sci. Eng. B 90 (2002) 34–37.